Evaluation of novel dendrimer–gold complex nanoparticles for theranostic application in oncology

Nevena Milivojević[1,2,3] (ID), Mariana R Carvalho[4,5] (ID), David Caballero[4,5] (ID), Snežana Radisavljević[6] (ID), Marija Radoičić[7] (ID), Marko Živanović[1,2,3] (ID), Subhas C Kundu[4,5] (ID), Rui L Reis[4,5] (ID), Nenad Filipović**[1,3,8] (ID) & Joaquim M Oliveira*[4,5] (ID)

[1]University of Kragujevac, Liceja Kneževine Srbije 1A, 34000, Kragujevac, Serbia
[2]Institute for Information Technologies, University of Kragujevac, Jovana Cvijića bb, 34000, Kragujevac, Serbia
[3]BioIRC – Bioengineering Research & Development Center, University of Kragujevac, Prvoslava Stojanovića 6, 34000, Kragujevac, Serbia
[4]3B's Research Group, I3Bs – Research Institute on Biomaterials, Biodegradables & Biomimetics, University of Minho, Headquarters of the European Institute of Excellence on Tissue Engineering & Regenerative Medicine, AvePark, Parque de Ciência e Tecnologia, Zona Industrial da Gandra, 4805-017, Barco, Guimarães, Portugal
[5]ICVS/3B's – PT Government Associated Laboratory, Braga/Guimarães, Portugal
[6]Faculty of Science, University of Kragujevac, Radoja Domanovića 12, 34000, Kragujevac, Serbia
[7]"Vinča" Institute of Nuclear Sciences, University of Belgrade, PO Box 522, 11000, Belgrade, Serbia
[8]Faculty of Engineering, University of Kragujevac, Sestre Janjić 6, 34000, Kragujevac, Serbia
*Author for correspondence: miguel.oliveira@i3bs.uminho.pt
**Author for correspondence: fica@kg.ac.rs

Aim: Despite some successful examples of therapeutic nanoparticles reaching clinical stages, there is still a significant need for novel formulations in order to improve the selectivity and efficacy of cancer treatment. **Methods:** The authors developed two novel dendrimer–gold (Au) complex-based nanoparticles using two different synthesis routes: complexation method (formulation A) and precipitation method (formulation B). Using a biomimetic cancer-on-a-chip model, the authors evaluated the possible cytotoxicity and internalization by colorectal cancer cells of dendrimer–Au complex-based nanoparticles. **Results:** The results showed promising capabilities of these nanoparticles for selectively targeting cancer cells and delivering drugs, particularly for the formulation A nanoparticles. **Conclusion:** This work highlights the potential of dendrimer–Au complex-based nanoparticles as a new strategy to improve the targeting of anticancer drugs.

Graphical abstract:
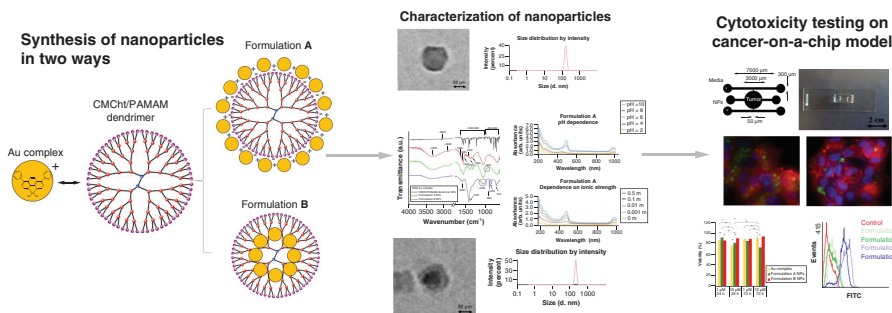
Taylor & Francis
Taylor & Francis Group

Cancer remains a major burden in our modern society, with many new cases being diagnosed every year [1]. In 2022, around 2 million new cancer cases and ∼600,000 cancer deaths were projected to occur in the USA. Epidemiologic estimations by the WHO put cancer as a leading cause of death by 2030 [2]. Cancer therapy faces serious challenges, particularly in drug discovery. The development and testing of new potential drugs through all preclinical and clinical phases can last years or even decades. It is estimated that the cost of developing one successful drug reaches US$1 billion, and out of 10,000 different compounds, only one gets approval for patient use [3].

Typically, anticancer drugs have been evaluated using reductionistic 2D assays or in animal models. However, as widely acknowledged, the 'flat' biology of 2D models is too simplistic to reproduce the complex structures and dynamics of the native tumor microenvironments. In these conditions, cancer cells respond to drugs significantly differently than *in vivo* [4]. Similarly, animal models have a weak correlation with human physiology, particularly the immune system. In addition, they are ethically controversial and highly expensive [5]. The combination of microfluidic tools and tissue engineering strategies has enabled the development of advanced, multifunctional platforms capable of re-creating the natural microenvironment of the tumor [6,7]. Such types of biochips are particularly well suited for investigating many of the dynamic events that can occur in the metastatic cascade, such as the efficacy of drugs when injected into the vasculature [8,9]. However, free drugs are highly unspecific, which threatens their efficacy [10,11]. In this regard, new strategies in cancer nanomedicine are also on the rise. Drug-carrying nanoparticles (NPs) can increase the specificity of the drug in the targeted location, reduce toxicity on healthy tissues, extend the half-life of the drug in circulation and reduce the amount and dose of the drug, making NPs a promising tools for targeted anticancer drug delivery [12,13]. Recent advances in nanotechnology have greatly impacted the field of medicine, leading to breakthroughs in areas such as prevention, diagnosis and therapy. This has resulted in the emergence of a new generation of nanomedicines. The utilization of modern nanoplatforms, which possess unique physicochemical properties, has the potential to revolutionize cancer treatment, as well as improve diagnostic and cell imaging techniques. These nanoplatforms represent a new class of tools in biomedicine that are designed for theranostic purposes [14].

The portfolio of NPs is vast, with a wide range of sizes, surface modifications, compositions and chemical properties. Among all the types of NPs, globular polymer molecules with an ethylenediamine nucleus and a polyamidoamine (PAMAM) branch, also known as dendrimers, have attracted attention in cancer research [15]. These dendrimers are biocompatible and nonimmunogenic, and their size can be effectively controlled by means of adjusting the number of branches. For example, G5 dendrimers, which are approximately 5–8 nm in size, have great therapeutic potential [14], since drugs of interest can be encapsulated within the cavities of dendrimers or covalently conjugated to them using a cleavable linker that is sensitive to specific conditions, such as acidic pH [16]. Acid-triggered drug-delivery systems are suitable for cancer treatment as they can respond to the slightly acidic microenvironment of tumors [17]. By means of modifying the surface of dendrimers with certain sugars, peptides, antibodies and other ligands such as hyaluronic acid and carboxymethyl-chitosan (CMCht), it is possible to create targeting agents that can bind to specific receptors on cancer cells [14].

On the other hand, the combination of PAMAM dendrimers, which have gained particular attention due to their unique properties, and gold (Au), which is the most commonly used inorganic material for biomedical purposes, has led to the development of nanohybrids that have the potential to revolutionize cancer therapy and diagnosis [14]. The ability of Au to absorb x-ray radiation makes it useful in cancer radiation therapy, and it can also be used as an imaging contrast agent in computed tomography diagnostics, in addition to its cytotoxic or photothermal effects [16,17]. Finally, CMCht/PAMAM dendrimers can serve as ideal vectors for various chemical compounds [18], offering great potential as intracellular drug carriers [19], particularly when they are combined with gold [20,21], and can be simultaneously used for both targeted chemotherapy and imaging diagnosis [17].

Research in the field of nano-oncology is currently focused on developing drug-delivery systems that are pH-responsive, have cytotoxic compounds and can transmit diagnostic information and monitor the therapeutic process *in situ* [16,17]. In this study, the authors synthesized anticancer dendrimer–Au complex-based nanoparticles through complexation and precipitation methods. A physicochemical characterization of NPs was carried out. The cytotoxicity screening and internalization of NPs by HCT-116 cells (human colon cancer cell line) were investigated *in vitro* using a biomimetic colorectal cancer-on-a-chip model. The use of organ-on-a-chip technology allows for simulation of the complex native microenvironment of colorectal cancer, providing a more accurate assessment

of the nanoparticles' efficacy. This research aims to contribute to the development of more effective and targeted cancer therapies.

Materials & methods

Synthesis of CMCht/PAMAM dendrimer NPs

The CMCht/PAMAM dendrimer NPs were prepared in a stepwise manner as described by Oliveira *et al.* [19]. PAMAM carboxylic acid-terminated dendrimers (G 1.5, 20% [w/v] methanolic solution) with an ethylenediamine core (Sigma, lot: MKBX0172V) were modified to increase the dendrimers' generation. To do this, an appropriate volume of PAMAM (G 1.5) in methanol was transferred to a volumetric flask and the solvent was evaporated under a N_2 atmosphere. The starting compound was then redissolved in ultrapure water to give a final concentration of 10 mgml^{-1} and the pH was adjusted to 6.5. Then, 1-ethyl-(3-dimethylaminopropyl) carbodiimide (EDC) hydrochloride (Sigma) was added to the solution at a molar ratio sufficient to modify the carboxylate residue of the dendrimers. The solution was kept under agitation for 30 min at room temperature to react. Ethylenediamine (Sigma) was added to the solution at a molar ratio equal to that of EDC and left to react for 4 h. After this period, the excess EDC was removed by dialysis (cellulose tubing, benzoylated for separating compounds with a MW ≤1200; Sigma). PAMAM-amine terminated compound was prepared as follows. CMCht with a degree of deacetylation of 80% and a degree of substitution of 47% was synthesized by a chemical modification route of chitin (Sigma) as previously described by Chen and Park [22]. Next, an exhaustive alkylation of the primary amines (Michael addition) was carried out. An appropriate volume of PAMAM-amine terminated was mixed with methanol (Sigma) and methyl methacrylate. CMCht/PAMAM dendrimer NPs were then precipitated after the addition of an appropriate volume of a saturated Na_2CO_3 (Sigma) solution and cold acetone (Pronalab). Precipitates were collected by filtration and dispersed in ultrapure water for dialysis throughout 48 h. Finally, CMCht/PAMAM dendrimer NPs were obtained by freezing the solution at -80°C and freeze-drying (TelstarCryodos-80) for 7 days to completely remove the solvent. Prepared in this way, the CMCht/PAMAM dendrimer NPs are water-soluble at physiological pH.

Labeling of CMCht/PAMAM dendrimer NPs with fluorescein isothiocyanate

The conjugates of CMCht/PAMAM-fluorescein isothiocyanate (FITC) were obtained by covalently bonding the amine group of CMCht and the isothiocyanate group of FITC (10 mg.ml^{-1} FITC [Sigma] in anhydrous dimethyl sulfoxide [Norconcessus]) to form a thiourea bond [23]. First, a 10 mg.ml^{-1} solution of CMCht/PAMAM dendrimer NPs was prepared in a carbonate–bicarbonate coupled buffer with pH 9.2. Then, a solution of FITC/dimethyl sulfoxide was added under agitation and kept in the dark at 4°C for 8 h. The FITC-labeled CMCht/PAMAM dendrimer NP solution was then dialyzed for 24 h against ultrapure water to remove unlinked FITC and filtered (pore size <220 nm) in sterile and dark conditions. The final product was obtained after freeze-drying.

CMCht/PAMAM dendrimer NP formulations with Au-complex

The Au-complex was synthesized as described by Radisavljević *et al.* [24] and incorporated into CMCht/PAMAM dendrimer NPs using two methods: complexation and precipitation. The positive charge of the Au-complex and the negative charge of the dendrimers provided an excellent basis for reaction. These two methods led to two different formulations of NPs:

- Formulation A: In the complexation method, Au-complex was mixed with CMCht/PAMAM dendrimer NPs (in equal molar quantities) in an aqueous solution for 24 h. The obtained product was then dialyzed against ultrapure water for 24 h, and the final solution was frozen at -80°C. The sample was obtained by freeze-drying.
- Formulation B: In the precipitation method, equal molar quantities of Au-complex and CMCht/PAMAM dendrimer NPs were dissolved in H_2O and mixed with a concentrated solution of Na_2CO_3. Then, cold acetone was added to allow NPs to precipitate. The obtained product was dialyzed against ultrapure water for 24 h, and the final solution was frozen at -80°C. The sample was obtained by freeze-drying.

Physicochemical characterization

The physicochemical characterization of the Au-complex and both NP formulations A and B are described below.

Dynamic light scattering

The particle size and ζ potential of the Au-complex and CMCht/PAMAM dendrimer formulations with Au were measured using a particle size analyzer (Zetasizer Nano ZS, Malvern Instruments). The particle size analyses were performed in an aqueous solution with low concentrations, using disposable sizing cuvettes. The electrophoretic determinations of ζ potential were investigated in water using the universal 'dip' cell at pH 7.4.

Transmission electron microscopy

The morphology of the newly synthesized NP formulations was examined using a Philips CM12 transmission electron microscope (Philips/FEI) equipped with the digital camera SIS MegaView III (Olympus). The samples were dissolved in water and placed on copper grids for observation. Images were obtained at a magnification of 35,000×.

Scanning electron microscopy & energy dispersive x-ray spectroscopy

Scanning electron microscopy imaging of both NP formulations and mapping characterization of Au-complex was done using a field emission scanning electron microscope equipped with energy dispersive x-ray spectroscopy – FEI Scios2, DualBeam system.

Adsorption efficiency

For assessing adsorption efficiency of both NP formulations, UV-visible spectrophotometry was done using a Multiskan SkyHigh UV/VIS Spectrophotometer (Thermo Fisher Scientific). Solutions of both NP formulations and Au-complex of known concentrations were prepared, spectra were recorded and calibration curves were obtained. Through the formula for calculating the concentration of unknown samples, the authors obtained the percentage of Au-complex in formulations A and B.

Fourier transform infrared

The dried Au-complex, CMCht/PAMAM dendrimer NPs and CMCht/PAMAM dendrimer NPs loaded with Au-complex (formulations A and B) were mixed with transparent potassium bromide (Sigma) and placed between two disks. A pressure of 4.5 metric tons was applied (using a Carver, Inc., press) on the disk to form a pellet. The spectrum of the formed pellet was measured by Fourier transform infrared (FTIR) spectroscopy (Exuinox 55, Bruker Optics, Inc.) in the range of 500–1800 cm^{-1}.

Stability of Au-complex + CMCht/PAMAM dendrimer NPs

The stability of CMCht/PAMAM dendrimer NPs + Au-complex formulations was analyzed using a UV-visible spectrophotometer. The stability was evaluated in terms of ionic strength and pH. The effect of ionic strength was evaluated 24 h after the addition of a solution of NaCl with final concentrations of 0, 0.001, 0.01, 0.1 and 0.5 M. The effect of pH was evaluated 24 h after adjusting the pH to 2, 4, 6, 8 and 10. The absorption spectra of freshly prepared, concentrated solutions of each type of NP were recorded using a Multiskan SkyHigh UV/VIS Spectrophotometer (Thermo Fisher Scientific).

Cell culturing

HCT-116 cells (human colon cancer cell line) were originally obtained from the American Collection of Cell Cultures. The cells were cultured under standard conditions (37°C in a humidified atmosphere, 5% CO$_2$) in Dulbecco's modified Eagle medium (DMEM; Gibco, Invitrogen) supplemented with 10% heat-inactivated fetal bovine serum (Alfagene) and 1% penicillin and streptomycin solution (Alfagene). The medium was replaced every 3 days. The subculture of cells was performed using 0.25% trypsin/EDTA (Gibco) for 5 min at 37°C before reaching 90% confluence in a cell culture flask.

Microfluidic chip design & fabrication

The microfluidic device was designed using computer-aided design software and replicated on a photolithography mask. The design included a central chamber for the encapsulation of cancer cells and two adjacent channels for the injection of NPs. The channels were connected to the central chamber through two micro-slits for the diffusion of cell culture medium and medium with treatment.

The microfluidic chip device was fabricated using standard UV- and soft lithography techniques. Briefly, a Si wafer (MicroChemicals) was heated for 15–30 min at 95°C. Next, a small volume of photo-resine (SU-8 2100,

Kayaku Advanced Materials) was deposited on top of the wafer and spin-coated at 500 rpm for 30 s to obtain a layer 180 μm thick. The wafer was then prebaked at 65°C and 95°C for 6 min and 37 min, respectively; UV-irradiated for 12 s; and postbaked at 65°C and 95°C for 5 min and 13.5 min, respectively. Finally, the nonexposed regions were removed (SU-8 Developer, Kayaku Advanced Materials) to release the mold. Next, polydimethylsiloxane (10:1 prepolymer:crosslinker; Sylgard™ 184 Dow®) was thoroughly mixed, poured into the mold and degassed in a vacuum chamber for 1 h and cured at 70°C for 3 h. The polydimethylsiloxane replica was gently detached, and the fluidic connection ports were punched. Finally, the polydimethylsiloxane replica and a clean glass slide were O$_2$ plasma-activated (200 W, 30 s) and bonded.

Microfluidic experiments

HCT-116 cancer cells were resuspended in Matrigel® at a density of 10×10^6 cells/ml^{-1} and then injected into the central chamber of the microfluidic device. The cells were incubated for 30 min at 37°C for crosslinking. Next, dendrimer NP–Au complex formulations A and B were added to the adjacent channels. As a control, DMEM medium was used. The cells were exposed to two different concentrations (1 and 10 μM) of both formulations for 24 or 72 h; 100 μl of both formulations for treated cells or medium for control cells was perfused through the lateral channels three times per day for the duration of the experiment.

Cell viability

Metabolic activity quantification

The metabolic activity of cells cultured within microfluidic chips was determined using the Alamar Blue assay (BioRad). This assay was performed in both the presence and absence of treatment. To retrieve encapsulated cells from Matrigel after 24 or 72 h, Corning Cell Recovery Solution (Laborspirit) was used for 60 min at 4°C. Once the cells were completely released from Matrigel, they were collected in a 1.5 ml Eppendorf tube and centrifuged to form a pellet at $300 \times$ g for 5 min at room temperature. Then, culture medium containing 20% (v/v) of Alamar Blue was added to the cell pellet and the mixture was incubated in the dark at 37°C in a CO$_2$ incubator. After the incubation period, 100 μl of the mixture was transferred to 96-well plates in triplicate, and the fluorescence was monitored at an emission wavelength of 590/20 nm (excitation wavelength 530/25 nm) using a microplate reader (Synergy HT, Bio-Tek Instruments). Medium with 20% v/v Alamar Blue was used as a blank.

Live/dead assay

The viability of cells cultured in microfluidic chips in the absence or presence of either formulation A or B was assessed using the live/dead assay. The side channels of the microfluidic chips were first washed with phosphate-buffered saline (PBS; Sigma), then incubated in the dark at 37°C in a solution of 1 μgml^{-1} calcein–acetoxymethylester (AM) and 5 μgml^{-1} propidium iodide prepared in DMEM for 30 min. After that, the samples were washed again with PBS and imaged by fluorescence microscopy (Axio Observer Zeiss).

Assessment of NPs' internalization efficiency

Fluorescence microscopy

To qualitatively assess the internalization of NPs, cells were seeded in the microfluidic device and cultured with 0.5 mgml^{-1} FITC-labeled Au-complex + CMCht/PAMAM dendrimer NPs under the previously described culture conditions for 24 and 72 h. The cells were then fixed using 4% formalin for 20 min at room temperature. The cell nuclei were stained with 4,6-diamidino-2-phenylindole, dilactate (Molecular Probes), while the F-actin filaments were stained using Texas Red-X phalloidin (Molecular Probes, Invitrogen) and imaged using fluorescence microscopy.

Flow cytometry

To quantitatively determine the internalization of NPs, flow cytometry analysis was performed. The cells were cultured in medium supplemented with 0.5 mg.ml^{-1} of FITC-labeled Au-complex + CMCht/PAMAM dendrimer NPs (both formulations) as previously described. After 24 and 72 h, cells encapsulated in Matrigel were retrieved using 500 μl of Corning Cell Recovery Solution (Corning) for 30 min at 4°C. The samples were then transferred to flow cytometry tubes, washed with 2 ml of 2% fetal bovine serum in PBS, centrifuged at 300 rpm for 5 min and resuspended in 1% formalin in PBS.
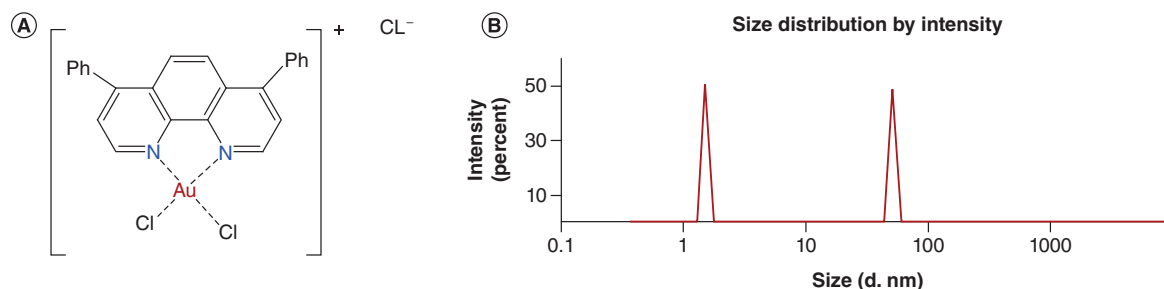
Figure 1.   (A) Molecular structure of the gold-complex and (B) size of the gold-complex (single and aggregates).

For the determination of cell viability, the same procedure was followed, as the cells were resuspended in 800 µl of 2% fetal bovine serum in PBS. Afterward, 5 µl of 7-aminoactinomycin D (Taper) was added to each sample for determining the number of dead cells. The cell suspensions were analyzed in the FACSCalibur flow cytometer (BD Biosciences).

Statistical analysis

Statistical analysis was done in IBM SPSS Statistics software (v23.0; IBM Corp., Armonk, NY, USA). Data were analyzed using the Shapiro–Wilk test of normality, one-way analysis of variance or the Kruskal–Wallis H test, respectively, and the two-tailed paired Student's t-test. All measurements were made in triplicate and the data are shown as mean $\pm$ SD. A p-value less than 0.05 was set to indicate statistical significance for a 95% CI.

Results

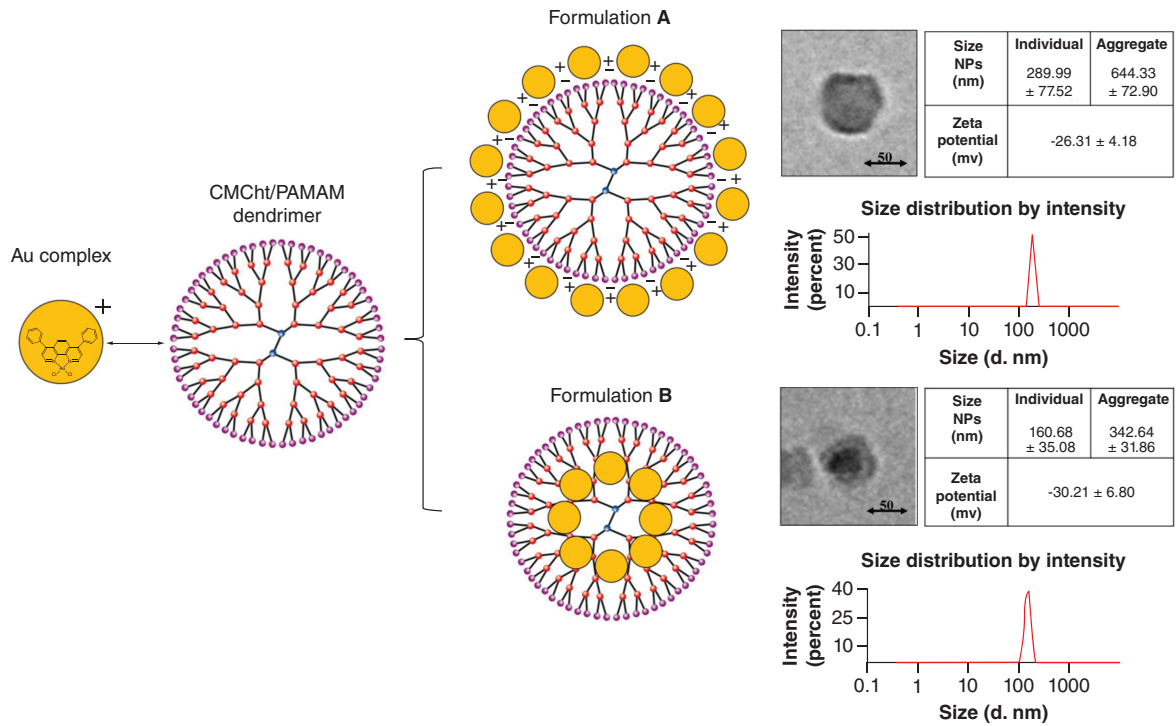### Characterization of the Au-complex & synthesized NP formulations A & B

Figure 1A depicts the molecular structure of the Au-complex with a diameter of 1.46 $\pm$ 0.49 nm (Figure 1B). The second peak observed at $\sim$50 nm corresponds to aggregated complexes. Regarding the ζ potential of the Au-complex, a positive charge of 32.30 $\pm$ 4.92 mV was obtained in water at neutral pH. This is noteworthy because CMCht/PAMAM dendrimer NPs themselves are negatively charged (-34.3 $\pm$ 3.0 mV in ddH$_2$0) [25].

Building on this characterization of the Au-complex, the authors synthesized two different NP formulations, A and B. The synthesis schemes and transmission electron microscopy images of both formulations are shown in Figure 2. It can be seen that formulation A NPs contain Au-complex on the periphery, while formulation B NPs contain Au-complex inside the cavities of the particle. For formulation A, it can be assumed that their interaction occurs on the surface, due to charge interactions, while in formulation B, the reaction occurs inside a particle that wraps around the Au-complex like a core.

The authors next measured the size and ζ potential of both formulations A and B in water at neutral pH. Both formulations A and B showed negative ζ values at -30.21 $\pm$ 6.80 mV and -26.31 $\pm$ 4.18 mV, respectively, thus indicating that the initial ζ potential shifted and negativity of the obtained NPs decreased as compared with the CMCht/PAMAM dendrimers. The particle size distribution of both formulations is depicted in Figure 2.

In the scanning electron microscopy images, one can see formulation A, where the dendrimer structures of the nanoparticle are clearly visible, while in formulation B, round, shrunken-shape nanoparticles can be seen because this formulation was synthesized by the precipitation method (Figure 3A & C). By analyzing the spectra obtained through energy dispersive x-ray spectroscopy analysis, the authors could detect the Au-complex on the surface of formulation A, while they did not detect it in formulation B due to the method of synthesis of such NPs (Figure 3B & D). Formulation B was obtained by precipitation, so in this way the Au-complex is encapsulated and the nanoparticle is closed, and for this reason it is not detected on the surface, but the Au-complex is only inside the NPs. Additionally, the percentage of gold-complex and adsorption efficiency of both formulations was done by UV-visible spectrophotometry. The percentage of Au-complexes in formulation A is 7.31%, while in formulation B it is 17.95%.

The characterization at the molecular level of the conjugate obtained by the coupling reactions of CMCht/PAMAM dendrimer with Au-complex was investigated by FTIR analysis. Figure 4 shows the FTIR spectrum of the Au-complex, the CMCht/PAMAM dendrimer NPs and the newly modified formulations of NPs (A and B, respectively). The obtained results are explained and discussed in the Discussion section.

Figure 2. Synthesis and morphology characterization of the newly synthesized nanoparticles. Synthesis scheme, representative transmission electron microscopy image, size and ζ potential and NP size distribution of formulation A and formulation B NPs.
NP: Nanoparticle.
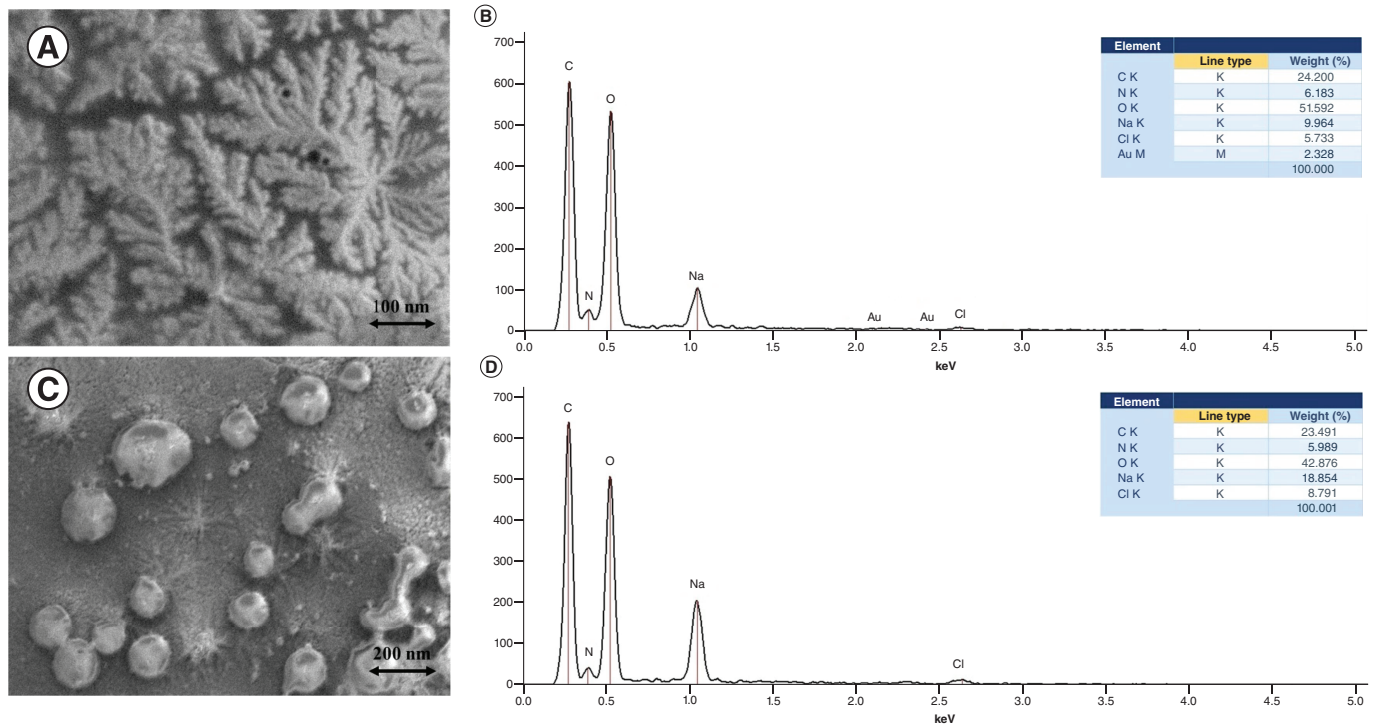
Figure 3.   (A) Scanning electron microscopy image of formulation A, (B) energy dispersive x-ray spectroscopy analysis of formulation A, (C) scanning electron microscopy image of formulation B and (D) energy dispersive x-ray spectroscopy analysis of formulation B.
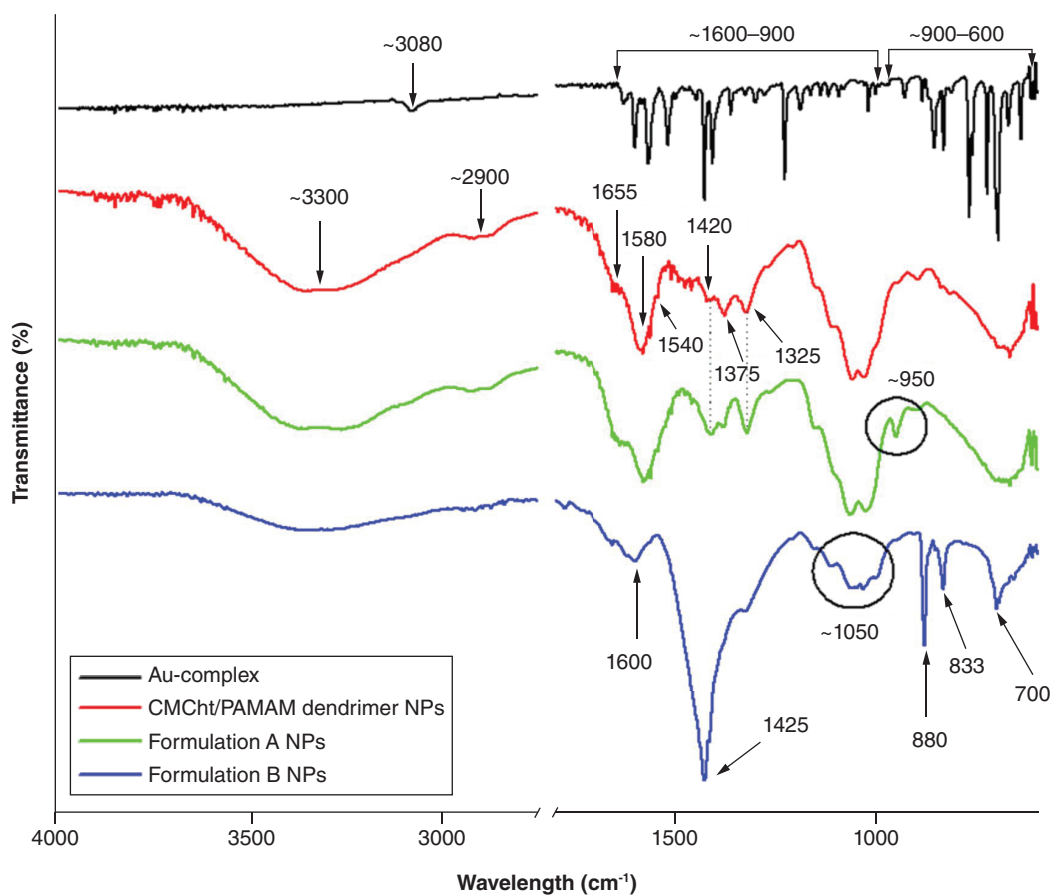
Figure 4.   Fourier transform infrared spectra of gold-complex, carboxymethyl-chitosan/polyamidoamine dendrimer nanoparticles and the newly modified formulations of nanoparticles (A & B).
NP: Nanoparticle.

The stability of the two formulations, A and B, against pH and ionic strength is shown in Figure 5. Both types of NPs were first dissolved in water at a certain ionic strength or pH value, and after 24 h the spectra were recorded. According to the UV-visible spectra, significant differences were observed in the spectra between both NPs regarding the influence of different ionic strengths and pH values. According to the results, the new NPs are stable at physiological pH values and strong ionic strength but are unstable in an acidic environment, such as in the native tumor microenvironment, which favors the release of the substance from the NPs.

Evaluation of NPs' efficacy in a microfluidic cancer-on-a-chip model

To evaluate the efficacy of the developed NPs, the authors developed an in-house microfluidic chip to investigate the NPs' interaction with human colorectal tumor cells seeded in Matrigel (Supplementary Figure 2). Briefly, the device contained three compartments: two lateral channels (each 300 µm in width and 180 µm in height) used to perfuse medium and NPs, and one circular, central chamber (3 mm in diameter and 180 µm in depth) where the HCT-116 cells were encapsulated, mimicking the tumor microenvironment. The channels and the chamber were interconnected through micro-slits that allowed the diffusion of media.

The possible cytotoxicity of the Au-complex and both formulations of newly synthesized NPs was assessed within the colorectal cancer-on-a-chip by measuring cellular metabolic activity (Figure 6) and proliferation (Supplementary Figure 3). HCT-116 cancer cells were exposed to the Au-complex and both types of Au-complex + CMCht/PAMAM NP formulations at two concentrations (1 µM and 10 µM) over a period of 24 and 72 h. As depicted in Figure 6, formulation A NPs displayed a significantly the best cytotoxic effect at a concentration of 10 µM after 72 h of culturing (p = 0.008; p = 0.007) compared to other treatments. Also, formulation A NPs showed better effect at a concentration of 1 µM after 72 h (p > 0.05) and a significantly better
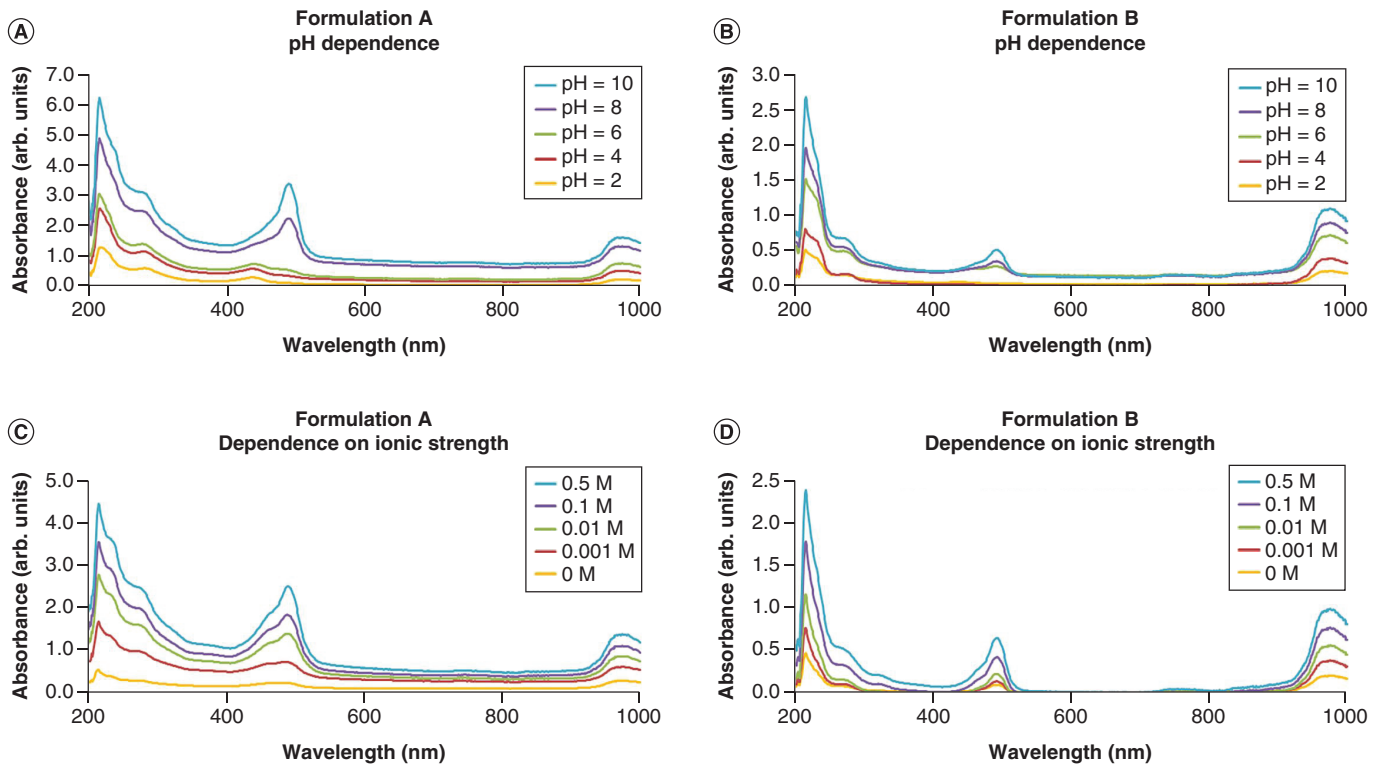
Figure 5.   Stability of newly synthesized formulations of nanoparticles. UV-visible spectrum of stability depending on the pH of **(A)** formulation A and **(B)** formulation B nanoparticles (NPs). UV-visible spectrum of stability depending on the ionic strength of **(C)** formulation A and **(D)** formulation B NPs.
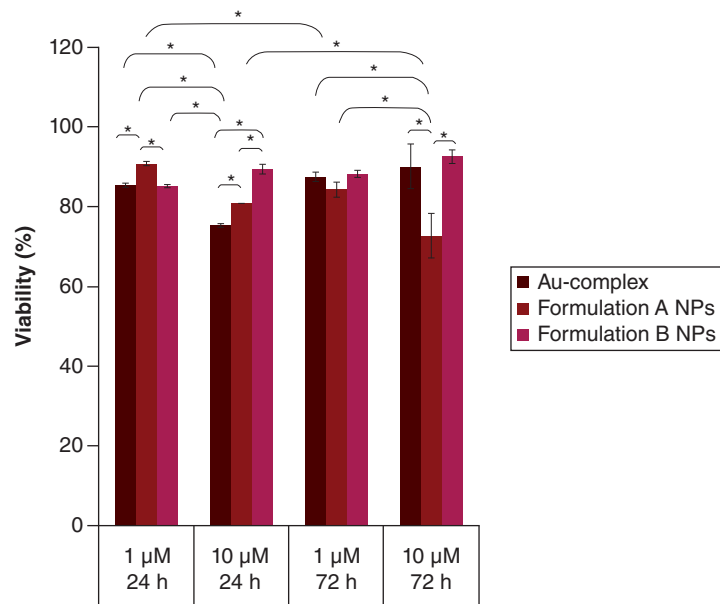
Figure 6.   HCT-116 cancer cell viability in the microfluidic device and statistical analysis depending on the applied concentration and treatment among themselves.
NP: Nanoparticle.

effect at a concentration of 10 μM after 24 h (p = 0.021). The formulation B NPs showed a significantly better effect than the formulation A NPs only after 24 h at a concentration of 1 μM (p = 0.003). In higher concentration and over time, there was no significant effect on cancer cell viability. Au-complex showed a significantly better effect than the modified NPs only after 24 h (p = 0.003; p = 0.042; p = 0.009, respectively), but later in time the cells recovered. Altogether, the formulation A NPs exhibited the best effect on HCT-116 colorectal cancer cells.
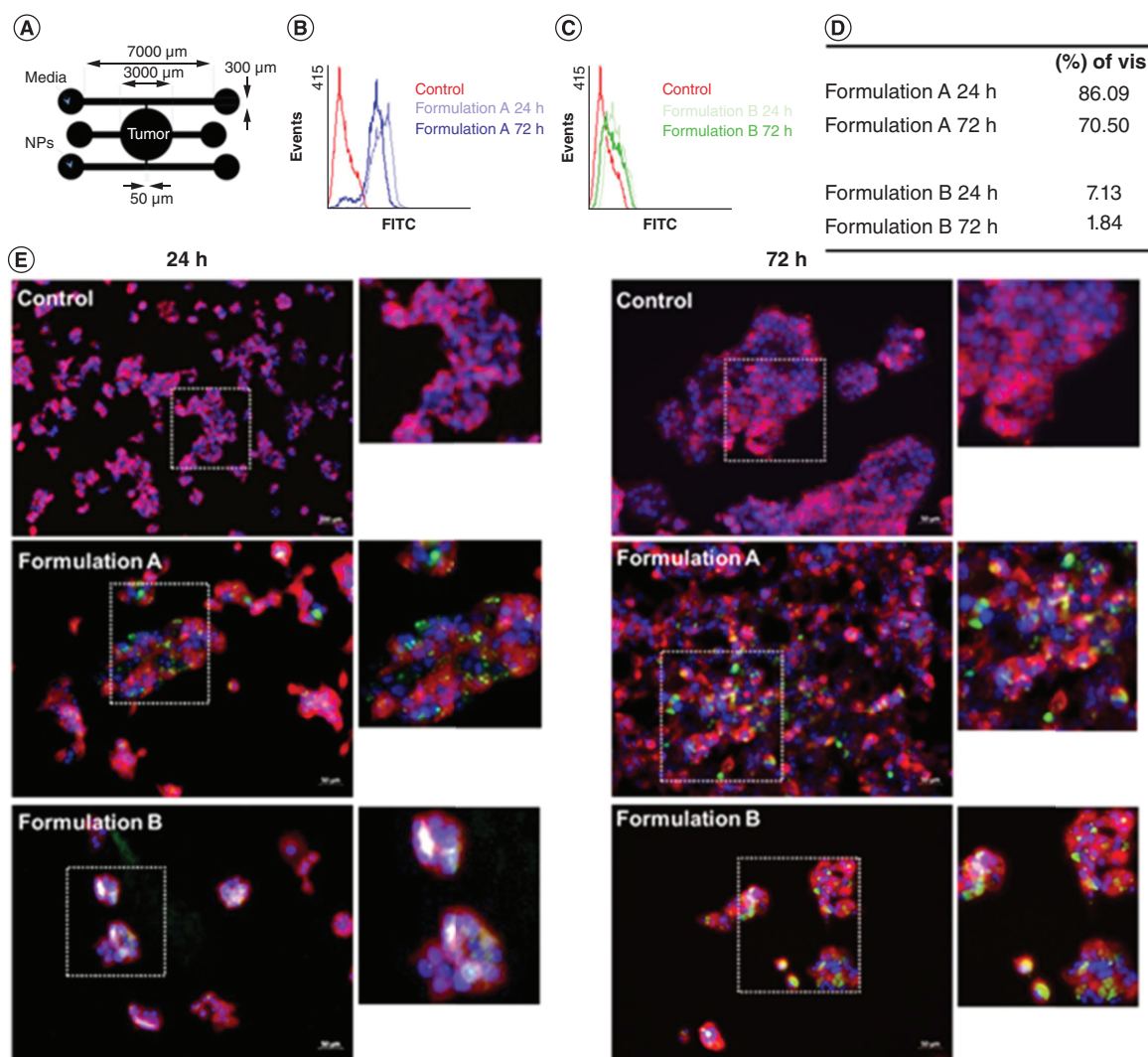
Figure 7.   Microfluidic assay of nanoparticle efficacy. (A) Scheme of the microfluidic chip and its building blocks. **(B)** Flow cytometry analysis of internalization of formulation A NPs. **(C)** Flow cytometry analysis of internalization of formulation B NPs. **(D)** Table of percentage of internalization of both NP formulations. **(E)** Fluorescence microscopy images of HCT-116 cancer cells stained for F-actin (phalloidin, in red) and nuclei (4,6-diamidino-2-phenylindole, dilactate, in blue) after treatment with formulation A and B NPs (in green) at 24 and 72 h. The upper row of images corresponds to untreated cells. Scale bar: 50 μm.
FITC: CMCht/PAMAM-fluorescein isothiocyanate; NP: Nanoparticle.

Representative fluorescence microscopy images obtained following the culture of cancer cells for 24 and 72 h with both types of FITC-labeled Au-complex + CMCht/PAMAM NP formulations are shown in Figure 7E. These images showcase that the NPs were either engulfed by the cells or located on their surfaces. A more quantitative assessment of the efficiency of NP internalization was conducted using flow cytometry analysis. The cellular uptake of both formulations of FITC-labeled NPs is depicted in Figure 7B & C. The internalization percentage of formulation A was significantly higher than that of formulation B (Figure 7D), as evidenced by the larger fluorescent signal in Figure 7B. Over time, the percentage of internalization for both NP formulations displayed a slight decrease, which is likely a result of cellular efflux mechanisms.

Discussion

The development of novel therapeutic nanoparticles is a crucial area of research in the field of cancer nanomedicine. These formulations have the potential to improve drug delivery and selectivity, enhancing the efficacy of chemotherapy. In this work, the authors focused on the development of new nanoparticle-based formulations and evaluated

their potential through the use of an in-house microfluidic chip device reproducing the physicochemical condition of the native colorectal tumor environment. The model was designed to facilitate efficient delivery of nanoparticles carrying the toxic complex and allowed for cell extraction after treatment, enabling the analysis the effects.

The authors developed novel nanoparticle formulations by combining the previously developed Au-complex [24] with CMCht/PAMAM dendrimer NPs in two different approaches. To gain more detailed information on the physicochemical characteristics of the obtained formulations, several tests were conducted. The particle size distribution indicated larger sizes than the dendrimer NPs alone (~50 nm) [19,22], indicating successful incorporation of the Au-complex. The formation of aggregate NPs can be attributed to the fact that during the synthesis of CMCht/PAMAM dendrimer NPs, more binding sites were available for crosslinking reactions [19].

The ζ potential value of the newly synthesized NP formulations, in water at a neutral pH, exhibited a slight negative charge (-30.21 ± 6.80 and -26.31 ± 4.18 mV), while the Au-complex itself had a positive charge (32.30 ± 4.92 mV). The CMCht/PAMAM dendrimers have negatively charged carboxymethyl groups distributed over their particle surfaces, resulting in a negative charge of -34.3 ± 3 mV [26]. The differences in charge between the dendrimer NPs and the dendrimers with an Au-complex (less negative) indicate a reduction in the number of carboxylic acid groups on the surface of the NPs, which is accompanied by an interaction with the Au-complex. This is confirmed by the results of FTIR analysis, where the structural characterization of individual components as well as obtained composite structures were identified, which demonstrated that the synthesis of modified NPs was successful in both approaches (Figure 4).

In the FTIR spectrum, the broad vibration band at ~3080 cm^{-1} is attributed to C–H stretching vibrations of pyridine rings of the Au-complex sample [24,27]. The bands obtained at 900–1600 cm^{-1} are assigned to the ring stretching vibrations of C–N, C=C, as well as ring stretching vibrations [28]. In addition, vibration bands between 600 and 900 cm^{-1} correspond to C–H in plane bending vibrations [27]. In the FTIR spectra of CMCht/PAMAM dendrimer nanoparticles, several bands are observed: broad band at ~3300 cm^{-1} corresponds to –O–H group, broad bands at ~2900 cm^{-1} correspond to N–H stretching vibration, band at 1655 cm^{-1} corresponds to C–O stretching vibration of amide I bond, band at 1580 cm^{-1} corresponds to C–N stretching and N–H bending vibration of amide II bond, band at 1540 cm^{-1} is attributed to C–N stretching vibration of amide II bond positioned inside dendrimer core, band at 1420 cm^{-1} corresponds to symmetric stretching mode of COO– group, band at 1375 cm^{-1} corresponds to asymmetric stretching mode of COO– group and band at 1325 cm^{-1} corresponds to C–N stretching vibration of amide III bond [19,27].

After the complexation process between Au-complex and dendrimer NPs, formulation A NPs were formed. In comparison with the molecular structure of the precursors, slight changes in the FTIR spectra of the formulation A NPs were obtained. Specifically, most of the present bands corresponded to the CMCht/PAMAM dendrimer NPs. However, a few variations in the vibrational spectra could be detected. The blueshift of the band at 1580 to 1573 cm^{-1} was observed, with an increase in the intensity of the bands at 1420 cm^{-1} and at 1325 cm^{-1}. Additionally, the formation of a new band at ~950 cm^{-1} was observed. These changes in the vibrational spectra could indicate potential surface modification of CMCht/PAMAM dendrimer NPs by the Au-complex. Specifically, the changes in the intensity of the bands that correspond to the symmetric stretching mode of the COO– group and C–N stretching vibration of amide II and amide III bond, as well as the formation of a new band, confirm a certain type of interaction between the individual components of the dendrimer and the Au-complex. On the other hand, after the precipitation process, significant changes in the chemical structures occurred. The presence of new bands in the FTIR spectra of the precipitated NPs at ~1600, 1425, 880, 833 and 700 cm^{-1} indicates the formation of new chemical bonds between the individual components during the multistep synthetic route. Specifically, the bands at ~1600 and 1425 cm^{-1} confirm the formation of a unidentate carboxylate complex that formed through the precipitation step of the synthesis [29]. The band that appeared at approximately 1600 cm^{-1} corresponds to the symmetric C–O stretching vibration, while the band at 1425 cm^{-1} corresponds to the C=O stretching vibration of the aforementioned complex. Additionally, the bands appearing at lower wavenumbers such as 880, 833 and 700 cm^{-1} are related to C–H in-plane bending vibrations that originate from the Au-complex precursor [24,26].

Transmission electron microscopy images revealed nanosphere-like shapes, single particles and aggregates in greater detail (Supplementary Figure 1). The dendrimer NPs themselves are also spherical in shape [19,30], and other examples of loaded NPs have retained the same shape after synthesis [25]. The Au-complex is incorporated into dendrimers in two ways: in formulation A NPs, the Au-complexes can be seen along the periphery of the particle, while in formulation B the Au-complex can be seen inside the cavities of the sphere.

According to the UV-visible spectra (Figure 5), at physiological pH values, the synthesized formulations of NPs exhibit stability, and peaks derived from Au-complexes (250–350 nm) [24] as well as FITC dye (488 nm) [25] can be clearly observed. Under basic conditions, the peaks are maintained but their absorbance is increased, while under acidic conditions, the peaks disperse. This is more pronounced in formulation A NPs and indicates the instability of this type of NP and the release of Au-complexes. This property of NPs is crucial, as the tumor microenvironment is typically acidic [31]. Therefore, the cytotoxic Au-complex will be released from the dendrimer NPs in the appropriate location. On the other hand, the biological environment in healthy tissue has a pH of about 7 and a strong ionic strength [29]. In terms of the influence of ionic strength, at higher values of salt concentration, stronger absorbance and clear peaks are obtained. At the highest examined ionic strengths, precipitation also occurred. In solutions of lower ionic strength (0.001 M and 0 M) of formulation A NPs, the peaks are flattened, while in formulation B NPs the peaks remain but are of lesser strength. According to these results, the NPs possess promising properties, as they show stability under the conditions necessary for distribution throughout the organism to the tumor environment.

Previous studies have shown that CMCht/PAMAM dendrimers have low cytotoxicity, and when labeled with FITC dye, they are stable for a long period of time without causing toxicity to cells [26]. The results of the present study indicate that the Au-complex has a weaker effect on 3D cell formation compared with 2D conditions, which is expected for most drugs [24,32]. Compared with the newly obtained NPs, the Au-complex has a weaker effect than formulation A after 72 h, which is significantly less after application of a higher concentration of these NPs (Figure 6). Formulation B NPs had the least cytotoxic effect in almost all conditions and time points, except after 24 h at a concentration of 1 μM, where it significantly reduced cell viability more than formulation A. Formulation A shows a cytotoxic effect that is both dose- and time-dependent. Also, formulation A in a dose of 10 μM after 72 h has statistically significantly the best effect of all three type of treatments.

To gain insight into the internalization of the new NPs into cells, the authors conducted fluorescence microscopy and flow cytometry experiments. As previously described, the size of the particles determines the mechanism of their internalization into the cell [33,34]. Cellular uptake of particles ~50 nm occurs through endocytosis, while larger particles are taken into the cytosol primarily by phagocytosis. Molecules smaller than 10 nm are inserted from the cytoplasm into the nucleus through the nuclear pore complex via passive diffusion [19,35]. Once NPs are internalized, they are degraded under the influence of enzymes or pH values within the endosome, thus increasing the availability of drugs or other substances within the cell [19]. In this way, CMCht/PAMAM dendrimer NPs increased the availability of cytotoxic Au-complex within colon cancer cells.

Fluorescence microscopy images show that HCT-116 cancer cells were able to internalize both types of NPs under dynamic conditions in a microfluidic chip device or to interact with particles on the surface. The images depict NPs distributed throughout the cytoplasm and even in the nucleus. Quantitative analysis revealed a much higher internalization of formulation A than formulation B NPs (Figure 7). Additionally, according to the results, internalization decreased with time; for both NPs, values were lower after 72 h. Similar data were obtained earlier on HCT-116 colon cancer cells, where internalization of their NPs reached a peak within 24 h and then decreased slightly [23]. So, it can be said that formulation A NPs show an increased cytotoxicity as compared with formulation B, especially statistically significant at a concentration of 10 μM (Figure 6), consistent with their internalization rates (Figure 7). In contrast, formulation B NPs show a saturation and recovery effect on cancer cells after 72 h, as seen by their proliferation at both final NPs' concentration of 1 and 10 μM (Figure 6).

Conclusion

In the field of nanomedicine, there is a pressing need to design and develop novel and more effective nanopharmaceuticals for cancer theranostics. Our study addresses this need by investigating the combination of novel nanoparticles as drug-delivery systems using a colorectal cancer-on-a-chip model. Our results demonstrated that dendrimer–gold complex-based nanoparticles obtained by complexation (formulation A) have a remarkable capability of targeting cancer cells and incorporating drugs. From a pharmaceutical perspective, the findings of incorporating toxic compounds into dendrimer nanoparticles have significant implications for real-world applications and hold potential for clinical translation. Overall, the combination of PAMAM dendrimers and gold has the potential to revolutionize cancer therapy and diagnosis by overcoming the challenges of traditional cancer treatments, as well as to pave the way for more personalized and effective therapies in the future.

Summary points

- This study addresses a pressing need to design and develop novel and more effective pharmaceuticals for cancer theranostics.
- Using a biomimetic cancer-on-a-chip model, the possible cytotoxicity of nanoparticles and their internalization by cancer cells can be evaluated.
- The results show promising capabilities of these nanoparticles for selective drug delivery.
- By internalizing these new carboxymethyl-chitosan/polyamidoamine dendrimer nanoparticles, the availability of cytotoxic gold-complex within colon cancer cells was increased.
- The combination of polyamidoamine dendrimers and gold has the potential to revolutionize cancer therapy and diagnosis.
- Comparison of two different methods of synthesis – complexation method (formulation A) and precipitation method (formulation B) – showed the advantages of synthesis by complexation.
- Quantitative analysis revealed much higher internalization of formulation A than formulation B nanoparticles.
- Nanoparticles based on dendrimer–gold complex as a new strategy have significant implications for real-world applications and hold potential for clinical translation.

Supplementary data

Author contributions

Financial disclosure

Competing interests disclosure

RL Reis is a member of the *Nanomedicine* editorial board, which was not involved in any editorial decisions related to the publication of this article, and all author details were blinded to the article's peer reviewers as per the journal's double-blind peer review policy. The authors have no other competing interests or relevant affiliations with any organization or entity with the subject matter or materials discussed in the manuscript apart from those disclosed.

Writing disclosure

No writing assistance was utilized in the production of this manuscript.

Open access

This work is licensed under the Attribution-NonCommercial-NoDerivatives 4.0 Unported License. To view a copy of this license, visit http://creativecommons.org/licenses/by-nc-nd/4.0/

References

Papers of special note have been highlighted as: ● of interest

1.   Mattiuzzi C, Lippi G. Current cancer epidemiology. *J. Epidemiol. Glob. Health* 9(4), 217–222 (2019).

2.   Siegel RL, Miller KD, Fuchs HE, Jemal A. Cancer statistics, 2022. *CA Cancer J. Clin.* 72(1), 7–33 (2022).

3.   Carvalho MR, Lima D, Reis RL, Oliveira JM, Correlo VM. Anti-cancer drug validation: the contribution of tissue engineered models. *Stem Cell Rev. Rep.* 13(3), 347–363 (2017).

4.   Horning JL, Sahoo SK, Vijayaraghavalu S *et al.* 3D tumor model for *in vitro* evaluation of anticancer drugs. *Mol. Pharm.* 5(5), 849–862 (2008).

5.   Jensen C, Teng Y. Is it time to start transitioning from 2D to 3D cell culture? *Front. Mol. Biosci.* 7, 33 (2020).

●   **Describes the advantages of 3D models compared with 2D monolayers and animal models.**

6.   Sittampalam S, Eglen R, Ferguson S *et al.* Three-dimensional cell culture assays: are they more predictive of *in vivo* efficacy than 2D monolayer cell-based assays? *Assay Drug Dev. Technol.* 13(5), 254–261 (2015).

7.   Carvalho MR, Lima D, Reis RL, Correlo VM, Oliveira JM. Evaluating biomaterial- and microfluidic-based 3D tumor models. *Trends Biotechnol.* 33(11), 667–678 (2015).

8.   Carvalho MR, Maia FR, Vieira S, Reis RL, Oliveira JM. Tuning enzymatically crosslinked silk fibroin hydrogel properties for the development of a colorectal cancer extravasation 3D model on a chip. *Glob. Chall.* 2(5–6), 1700100 (2018).

9.   Carvalho MR, Barata D, Teixeira LM *et al.* Colorectal tumor-on-a-chip system: a 3D tool for precision onco-nanomedicine. *Sci. Adv.* 5(5), eaaw1317 (2019).

●   **Describes a tumor-on-a-chip platform that enables precise delivery of nanomedicines, cytotoxicity assays and relevant gene expression analysis.**

10.   Bhatia SN, Ingber DE. Microfluidic organs-on-chips. *Nat. Biotechnol.* 32(8), 760–772 (2014).

11.   Kasendra M, Tovaglieri A, Sontheimer-Phelps A *et al.* Development of a primary human small intestine-on-a-chip using biopsy-derived organoids. *Sci. Rep.* 8(1), 2871 (2018).

12.   Haley B, Frenkel E. Nanoparticles for drug delivery in cancer treatment. *Urol. Oncol.* 26(1), 57–64 (2008).

13.   Palmerston Mendes L, Pan J, Torchilin V. Dendrimers as nanocarriers for nucleic acid and drug delivery in cancer therapy. *Molecules* 22(9), 1401 (2017).

14.   Kesharwani P, Choudhury H, Meher JG, Pandey M, Gorain B. Dendrimer-entrapped gold nanoparticles as promising nanocarriers for anticancer therapeutics and imaging. *Prog. Mater. Sci.* 103, 484–508 (2019).

●   **The authors describe the use in theranostic applications of nanoparticles that are a combination of dendrimers and gold as next-generation nanomedicine.**

15.   Carvalho MR, Reis RL, Oliveira JM. Dendrimer nanoparticles for colorectal cancer applications. *J. Mater. Chem. B* 8(6), 1128–1138 (2020).

16.   Mignani S, Shi X, Ceña V, Rodrigues J, Tomas H, Majoral JP. Engineered non-invasive functionalized dendrimer/dendron-entrapped/complexed gold nanoparticles as a novel class of theranostic (radio)pharmaceuticals in cancer therapy. *J. Control. Rel.* 332, 346–366 (2021).

●   **The authors show the concept of using nanoparticles based on dendrimers and containing gold for theranostic purposes. These nanoparticles cover several aspects such as targeted imaging, drug delivery and radiotherapy.**

17.   Zhu J, Wang G, Alves SC *et al.* Multifunctional dendrimer-entrapped gold nanoparticles conjugated with doxorubicin for pH-responsive drug delivery and targeted CT imaging. *Langmuir* 34(41), 12428–12435 (2018).

18.   Oliveira JM, Salgado AJ, Sousa N, Mano JF, Reis RL. Dendrimers and derivatives as a potential therapeutic tool in regenerative medicine strategies – a review. *Prog. Polym. Sci.* 35(9), 1163–1194 (2010).

19.   Oliveira JM, Kotobuki N, Marques AP *et al.* Surface engineered carboxymethylchitosan/poly(amidoamine) dendrimer nanoparticles for intracellular targeting. *Adv. Funct. Mater.* 18(12), 1840–1853 (2008).

20.   Li X, Kono K. Functional dendrimer–gold nanoparticle hybrids for biomedical applications. *Polym. Int.* 67(7), 840–852 (2018).

21.   Saw WS, Anasamy T, Anh Do TT *et al.* Nanoscaled PAMAM dendrimer spacer improved the photothermal-photodynamic treatment efficiency of photosensitizer-decorated confeito-like gold nanoparticles for cancer therapy. *Macromol. Biosci.* 22(8), e2200130 (2022).

22.   Chen XG, Park HJ. Chemical characteristics of O-carboxymethyl chitosans related to the preparation conditions. *Carbohyd. Polym.* 53(4), 355–359 (2003).

23.   Carvalho MR, Maia FR, Silva-Correia J, Costa BM, Reis RL, Oliveira JM. A semiautomated microfluidic platform for real-time investigation of nanoparticles' cellular uptake and cancer cells' tracking. *Nanomedicine* 12(6), 581–596 (2017).

•   **This work demonstrates that a microfluidic-based platform enables real-time monitoring of cellular uptake and evaluation of drug release effects.**

24.   Radisavljevic S, Dekovic Kesic A, Cocic D *et al.* Studies of the stability, nucleophilic substitution reactions, DNA/BSA interactions, cytotoxic activity, DFT and molecular docking of some tetra- and penta-coordinated gold(III) complexes. *New J. Chem.* 44(26), 11172–11187 (2020).

25.   Carvalho MR, Carvalho CR, Maia FR *et al.* Peptide-modified dendrimer nanoparticles for targeted therapy of colorectal cancer. *Adv. Ther.* 2(11), 1900132 (2019).

26.   Socrates G. *Infrared and Raman Characteristic Group Frequencies: Tables and Charts.* John Wiley & Sons Ltd, Chichester, England (2001).

27.   Salgado AJ, Oliveira JM, Pirraco RP *et al.* Carboxymethylchitosan/poly(amidoamine) dendrimer nanoparticles in central nervous systems-regenerative medicine: effects on neuron/glial cell viability and internalization efficiency. *Macromol. Biosci.* 10(10), 1130–1140 (2010).

28.   Maschmeyer I, Lorenz AK, Schimek K *et al.* A four-organ-chip for interconnected long-term co-culture of human intestine, liver, skin and kidney equivalents. *Lab. Chip* 15(12), 2688–2699 (2015).

29.   Song W, Duan W, Liu Y *et al.* Ratiometric detection of intracellular lysine and pH with one-pot synthesized dual emissive carbon dots. *Anal. Chem.* 89(24), 13626–13633 (2017).

30.   Vieira S, Vial S, Maia FR *et al.* Gellan gum-coated gold nanorods: an intracellular nanosystem for bone tissue engineering. *RSC Adv.* 5(95), 77996–78005 (2015).

31.   Boedtkjer E, Pedersen SF. The acidic tumor microenvironment as a driver of cancer. *Annu. Rev. Physiol.* 82, 103–126 (2020).

32.   Imamura Y, Mukohara T, Shimono Y *et al.* Comparison of 2D- and 3D-culture models as drug-testing platforms in breast cancer. *Oncol. Rep.* 33(4), 1837–1843 (2015).

33.   Bannunah AM, Vllasaliu D, Lord J, Stolnik S. Mechanisms of nanoparticle internalization and transport across an intestinal epithelial cell model: effect of size and surface charge. *Mol. Pharmaceut.* 11(12), 4363–4373 (2014).

34.   Wu M, Guo H, Liu L, Liu Y, Xie L. Size-dependent cellular uptake and localization profiles of silver nanoparticles. *Int. J. Nanomed.* 14, 4247–4259 (2019).

•   **The results and conclusions of this study are very important to understand the exact mechanism of interaction between nanoparticles and cells. They show the endocytic pathways of nanoparticles to provide delivery of medicines.**

35.   Petithory T, Pieuchot L, Josien L, Ponche A, Anselme K, Vonna L. Size-dependent internalization efficiency of macrophages from adsorbed nanoparticle-based monolayers. *Nanomaterials (Basel)* 11(8), 1963 (2021).